

Focal mechanism of Badr earthquake, Saudia Arabia of August 27, 2009

Khalid S. Aldamegh · Hesham Hussein Moussa ·
S. Nasser Al-Arifi · Sayed S. R. Moustafa ·
Moustafa Hemeda Moustafa

Received: 9 June 2010 / Accepted: 21 September 2010 / Published online: 14 October 2010
© Saudi Society for Geosciences 2010

Abstract Focal mechanism solution of the 27th August 2009 earthquake ($m_b=4.0$) that occurred in the Badr area, northwest of Saudi Arabia, approximately 50 km from the Red Sea has been determined from the P-wave first motion polarities. Results show normal faulting mechanism with a negligible component of strike-slip motion with NE T -axis direction. This type of mechanism is common with other earthquakes of the northwestern Saudi Arabia and is considered to present the tectonic movement of the region. The dominantly extensional tectonic regime in this province demonstrates the influence of NE extension in the Red Sea. The strikes of the solution are consistent with those of the main faults near the epicenter. Hypocentral location of this earthquake was carried out using the data from the King Abdulaziz City of Science and Technology Seismic Network, Saudi Arabia, and the Egyptian National Seis-

mological Network, Egypt. The horizontal and vertical confidence estimates are 0.5 km for both. The local magnitude, M_L , following the Richter's original definition was also derived from ten digital three-component broadband seismograms. The average local magnitude determined in this study is 3.8 ± 0.17 . The estimated seismic moment of this event is $3.7e + 14 \text{ Nm}$ ($M_W = 3.66 \pm 0.07$).

Keywords Focal mechanism · Badr earthquake · Moment magnitude · Seismotectonics

Introduction

On 27th August 2009, at 20:22 (UTC), a small magnitude earthquake ($m_b=4.0$; International Data Center (IDC), 18 stations), occurred in Badr area, approximately 50 km from the Red Sea (Fig. 1). The catalog of Ambraseys et al. (1994) lists two historical earthquakes within 60 km distance from the Badr earthquake (Fig. 2). The two events have moderate size earthquakes; 626 and 1,256. The first one was felt at Mt. Uhud outside Al-Madinah Almonawarah. The second event is associated with an extensive eruption, occurred close to the city of Medina. The Badr earthquake is located in an area of relatively low seismic activity (Fig. 2). Two recent earthquakes occurred on 22th June 2004 ($M_w=5.1$) near Tabuk and on 19th May 2009 ($M_w=5.7$) in Al Ais. Both of them are located NW of Badr earthquake, in the Arabian Shield and close to the Red Sea (Fig. 1). The focal mechanism solutions of the two earthquakes show pure normal faulting mechanism with the two nodal planes oriented NW-SE, parallel to the Red Sea (Aldamegh et al. 2009 and the Centroid Moment Tensor Catalog, Harvard Seismology, <http://www.seismology.harvard.edu/CMTsearch.html>). The strike of the fault planes agrees well with the surface observations of NW trending faults, interpreted to be a part of a Najd Fault System. The

K. S. Aldamegh · M. H. Moustafa
Astronomy and Geophysics Research Institute,
King Abdulaziz City for Science and Technology (KACST),
Riyadh, Saudi Arabia

H. Hussein Moussa (✉) · S. S. R. Moustafa
Seismology Department,
National Research Institute of Astronomy and Geophysics,
Helwan, Egypt
e-mail: hesham6511421@yahoo.com

H. Hussein Moussa · S. N. Al-Arifi · S. S. R. Moustafa
Community College, Shaqra University,
Alquwayiyah, Saudi Arabia

H. Hussein Moussa
North Africa Seismological Group NASG Net40/OEA/ICTP,
Trieste, Italy

S. N. Al-Arifi
Geology Department, Faculty of Science, King Saud University,
Riyadh, Saudi Arabia

stress field of the Tabuk and Al Ais events is characterized by a nearly horizontal NE-SW extension.

In this work, we present the locations of 27th August 2009 Badr earthquake using the integrated data of local and regional seismic networks of Egypt and Saudi Arabia. The main scope of this paper is to address the focal mechanism solution of 27th August 2009 Badr earthquake and to determine the local magnitude (M_L) and moment magnitude of this event. Studying the source mechanism is necessary for improving our understanding of the seismotectonics into this region and discussing its regional implications. Badr earthquake used to obtain information about the stress field in the Red Sea margin and to compare it with the results obtained from the 22th June 2004 ($M_w=5.1$) Tabuk and the 19th May 2009 ($M_w=5.7$) Al Ais earthquakes. The correlation between the earthquakes and faults in the source area has been discussed. The results coming from present-day stress field studies give important contribution to seismic hazard assessment.

Geological setting

Geologically, the area of this event is located in the Hijaz microplate (terrane) which is one of the five terranes forming the Arabian Shield (Fig. 1; Vail 1983; Camp 1984; Stoesser et al. 1984). These “terrane” are now separated by major, mainly N-S and NE-SW, suture zones lined by serpentized ultramafic rocks (ophiolites and tectonic slices). They are interpreted as recording the formation of island-arc crust or continental-marginal-arc crust above complexity evolving subduction systems during the Late Proterozoic.

The Precambrian Arabian Shield is separated by the Red Sea rift from its counterpart, the Nubian Shield of Egypt and Sudan. Approximately 81,000 km² of the shield area are overlain by extensive Tertiary and Quaternary basaltic lava fields (harrats). Their distribution is related to the intense brittle tectonics (fracturing/faulting) associated with the opening of the Red Sea, which began at the end of the Oligocene or beginning of the Miocene (about 25 Ma), when the Arabian and African continental blocks were forced apart (Stoesser 1986). Tensional stress caused substantial subsidence along the axis of the Red Sea and its margins, and the extension fissures became conduits for basaltic magma; dikes of gabbro and dolerite running subparallel to the axis of the Red Sea at the western margin of the Arabian Shield originated as fissures filled with basic magma that crystallized at depth, but are now visible in outcrop due to subsequent erosion. Eruptions have occurred from the Miocene (25 Ma) to the present (several eruptions are recorded in historical time). Most of the magma reached the surface and formed extensive flows that make up the basaltic plateaus (harrats). The last eruption was from Harrat Rahat in 1256 AD, when the lava flow stopped short of the gates of Al-Madinah (Camp et al. 1987).

The Arabian Shield is characterized by the existence of large size faults forming a belt with a width of 300 km and a length of 1,100 km. They cut the Arabian Shield from southeast to the northwest (Najd fault system). The Najd fault system took place during the last part of the 530–630-m.y. period (Stern 1985). It is considered to be the latest tectonic event in the formation of the Arabian Shield which may be formed due to the east–west stress regime (Delfour

Fig. 1 Structural features of Arabian Shield (Johnson 1983). (a) Midyan terrane, (b) Yanbu suture, (c) Hijaz terrane, (d) Asir terrane, (e) Bir Umq suture, (f) Nabitah orogenic belt, (g) Afif terrane, (h) Al Amar suture, (i) Ar Rayn terrane, (k) tertiary basalt (harrats); red circle location of Badr, Tabuk, and Al Ais earthquakes. Blue filled squares location of the seismological stations. Hexagons location of Badr. Black lines Najd fault system. Red color patches ophiolite suite

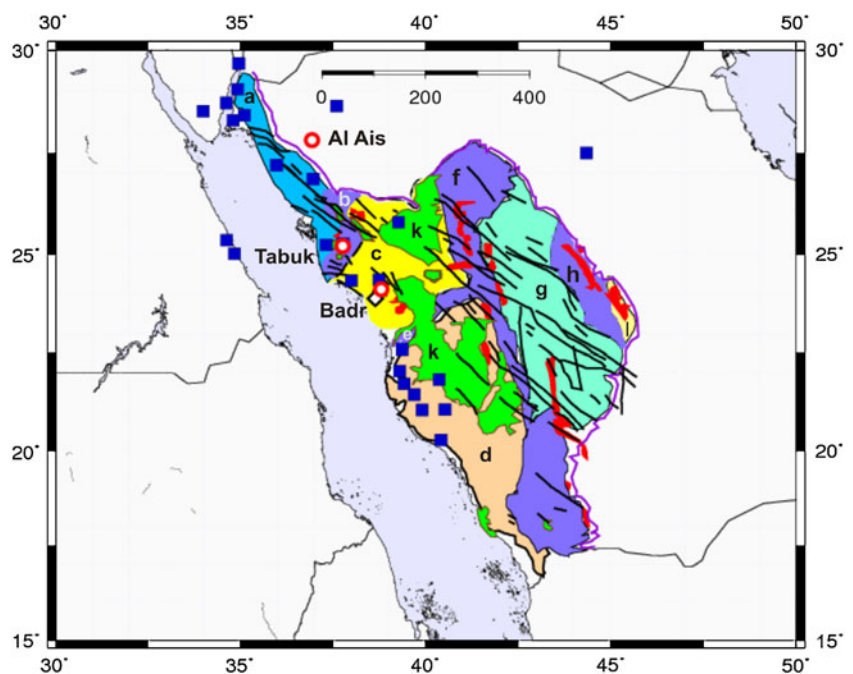
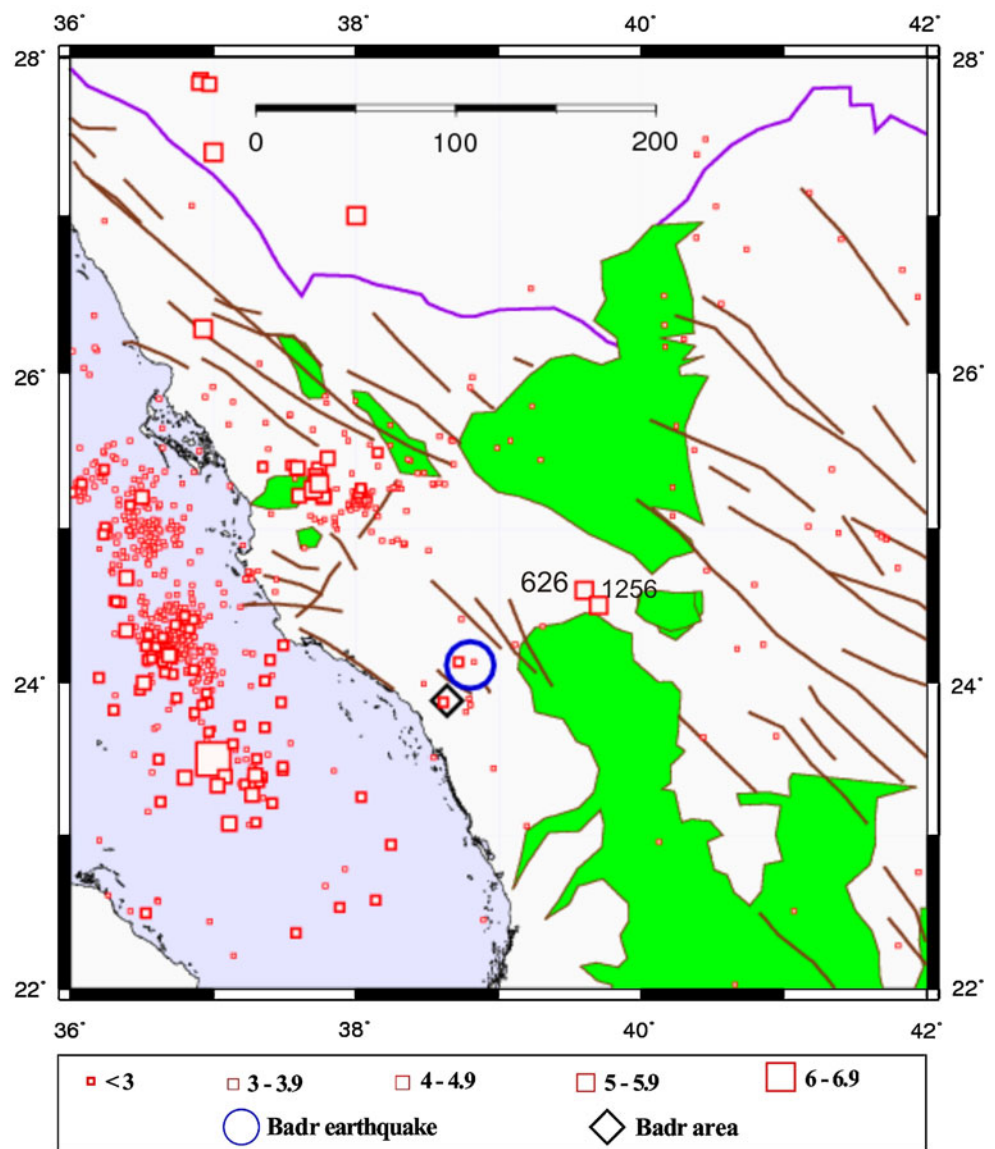


Fig. 2 Seismicity of the studied area from 1900 to 2009 in addition to the historical earthquakes



1983). They trend northwest. They are left-lateral strike-slip faults that either followed or cut across the margins of the Pan African structures (Stern 1985).

Station and waveform data

The waveform data collected for this study comprises all the available records of 27th August 2009 Badr earthquake from the King Abdulaziz City of Science and Technology Seismic Network (KACST), Saudi Arabia (Fig. 1). The current KACST network consists of three component broadband stations. Some short-period digital waveforms were also requested from the Egyptian National Seismological Network, Seismology Department, National Research Institute of Astronomy and Geophysics, Helwan, Egypt (Fig. 1).

Hypocentral determination

To determine the hypocenter location of Badr earthquake, we picked the phase data from the digital broadband waveforms recorded by the seismological network of King Abdulaziz City of Science and Technology Seismic Network. We improved the accuracy of hypocenter location by adding some phase data from the Egyptian National Seismological Network. The location was obtained using P arrival times of 24 stations and six S-wave arrival times. The P and S onset times were individually picked to be within 0.1 s. This event was relocated from the 2009 August data set with HYPOINVERSE software (Klein 1987) which, unlike VELEST, also calculates the standard errors in the hypocentral parameters and the velocity model of Rodgers et al. (1999). The parameters of this earthquake are shown in Table 1. The locations of this event and the

Table 1 Location parameters for the 27th August 2009 earthquake

Date	OT	Latitude (°)	Longitude (°)	Depth	RMS	ERH	ERZ
Y M D	H M S			km	s	km	km
2009 08 27	20 22 27.02	24.1188	38.7905	12.24	0.12	0.56	0.50

seismic stations used to locate it are shown in Fig. 1. On the basis of the location process, the estimated error in both epicentral error (ERH) and depth error (ERZ) equals to 0.56 km and 0.50, respectively, while the mean root square residual is 0.12. This event took place at a shallow depth of about 12.24 km.

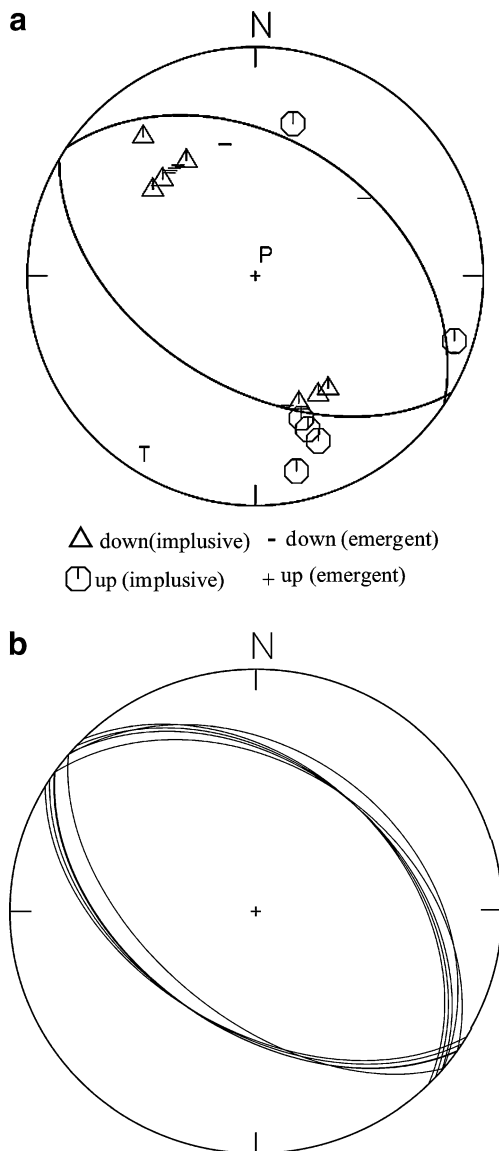


Fig. 3 a Lower hemisphere equal area projections of the focal sphere for Badr earthquake, letter symbols indicate the position of compressional (*P*) and tensional (*T*) axes. b The range of focal mechanisms that satisfied the chosen error limits

Focal mechanism

We read the impulsive first motion directions from the waveform data of KACST using SAC software. P-wave onset is distributed uniformly and well-defined at stations. The focal mechanism solution of Badr event was determined from the first motion polarities. Double-couple focal mechanism solution for this event was determined using the grid search program FOCMEC that provides the best fit of a given set of first motion polarities observed for an earthquake (Snoke 2003). The input data includes polarities, station azimuth, and P-wave take-off angles at the source. The azimuths and take-off angles corresponding to the epicentral distance and focal depth were computed using the velocity model of Rodgers et al. (1999). The output of the program was acceptable fault plane solution that is based on the selection criteria for the number of polarity errors. The selection criteria for both polarities and angles allow correction or weightings for near-nodal solutions. The best-fitting focal planes of the earthquake are plotted on an equal area lower hemisphere projection (Fig. 3a) while the focal parameters are summarized in Table 2. Figure 3b shows the range of fault planes that satisfy the first motion observations described above. First motion polarities from P-waves recorded at 21 stations with epicentral distances $\Delta < 700$ km are compatible with this solution. The computed fault plane solution belongs mostly to pure normal faulting mechanism. The obtained stress field shows a NE-SW extension with horizontal *T*-axis (Plunge 4).

Local magnitude determination

The average local magnitude of Badr earthquake was calculated using the digital waveforms recorded at the broadband stations of KACST. To determine M_L of Badr earthquake, synthetic Wood–Anderson (W-A) seismograms were calculated by removing the instruments response of each recording and convolving the displacement ground

Table 2 Source mechanism parameters for the 27th August 2009 earthquake

Plane 1			<i>P</i> -axis		<i>T</i> -axis	
Strike	Dip	Slip	Trend	Plunge	Trend	Plunge
304.16	40.87	-87.33	09.91	85.49	212.77	04.16

motion with the theoretical response of a Wood–Anderson seismometer; period = 0.8 s, magnification = 2,800, and damping = 0.8 (Richter 1935). M_L was obtained from the maximum trace amplitude into these synthetic W-A seismograms, using Richter (1958) amplitude–distance corrections. The maximum observed NS and EW amplitude values were averaged to constitute a single measurement $\sqrt{(ns^2 + ew^2)}$. Following the method originally used by Richter (1935, 1958), M_L is given by the following equation:

$$M_L = \log A - \log A_0 \tag{1}$$

where A is the maximum trace amplitude in millimeters measured from a Wood–Anderson seismogram, A_0 is a distance-dependent attenuation curve. M_L can be corrected for the difference $\delta \log A_0$ in the attenuation properties between our region of interest and southern California, where M_L was developed, using the equation of Ebel (1982):

$$\delta \log A_0 = \log(\exp((\gamma_{sc} - \gamma_{ss})\Delta)) \tag{2}$$

where γ_{sc} is the spatial attenuation coefficient appropriate for southern California, γ_{ss} is the attenuation coefficient for the Arabian Shield. Δ is the source to receiver distance. Determining the corrections factor $\delta \log A_0$, the formula of the local magnitude takes the form:

$$M_L = \log A - \log A_0 - \delta \log A_0 \tag{3}$$

Nuttli (1973) showed that the value of $\gamma_{sc} = 0.0054$ for southern California while γ_{ss} for the Arabian shield equals to 0.0016 at about 1 Hz (Sandvol et al. 2007). Table 3 shows the values of the correction factors for A_0 in the local magnitude formula according to the new value of γ_{ss} . We find that the average corrected local magnitude, M_L , of the 27th August 2009 earthquake estimated from ten stations is 3.8 ± 0.17 . This value is nearly equal to the local magnitude estimated by three stations of the IDC.

Seismic moment and moment magnitude

Seismic moment (M_o) and the moment magnitude (M_w) were also estimated from the displacement spectra of the Lg phase for the Badr earthquake. The analyzed data consist of four vertical component broadband records characterized by good signal-to-noise ratio and were located within epicentral distances ranging from 27 to 235 km. First, the signal was corrected to zero baseline and the instrumental

Table 4 Moment and moment magnitude from four broadband stations

St. code	Δ (km)	Ω_0 (ms)	M_o (Nm)	M_w
YOBS	27	0.62e-05	3.0e14	3.60
FRJS	179	0.86E-06	3.1e14	3.62
KBRS	191	1.20e-06	4.0e14	3.70
KHLS	235	0.98e-06	4.3e14	3.74

response. A cosine taper was applied to the selected signal window. The observed Lg amplitude spectrum was calculated for a selected signal window ranging from 4 to 6 s. Lg-wave attenuation along the path was taken into account by a quality factor of 560 (Sandvol et al. 2007). Assuming an omega-square Brune’s source model, the low-frequency spectral amplitude Ω_0 is estimated using the nonlinear least-squares inversion techniques. Values are given in Table 4. The following relations and parameters were used to derive the seismic moment from the Lg-wave low-frequency spectral amplitude Ω_0 (Street et al. 1975).

$$M_o = 4\pi\rho\beta^3Ro(R/R_o)\Omega_0, \quad \text{for } R < R_o \tag{4}$$

$$M_o = 4\pi\rho\beta^3Ro(R/R_o)^{1/2}\Omega_0, \quad \text{for } R \geq R_o \tag{5}$$

where ρ is the density of the medium in gram per cubic centimeter, β is the shear wave velocity in kilometers per second, R is the epicentral distance in kilometers, and Ω_0 is the low-frequency spectral level of the Lg-wave selected window. R_o is used to account for different kind of Lg-waves geometrical spreading. Constant values corresponding to the source region in Eqs. 4 and 5 were assumed as follows $\rho=2.7 \text{ gm/cm}^3$, $\beta=3.5 \text{ km/s}$, and $R_o=100 \text{ km}$. The estimated seismic moments and moment magnitudes for the studied event are listed in Table 4 whereas an example of the fitted displacement spectra at KBRS station is plotted in Fig. 4. The average seismic moment and moment magnitude derived from the displacement spectrum of the four broadband stations are $3.7e+14 \text{ Nm}$ and 3.66 ± 0.07 , respectively

Discussion and conclusions

The Arabian is bounded within a small area of the globe, by the three principal types of plate boundaries (Beydoun 1994):

Table 3 The values of $\delta \log A_0$ for the different distances according to the new value of γ_{ss}

Δ	25	50	75	100	125	150	175	200	225	250	275	300	325	350	375	400
$\delta \log A_0$	0.04	0.08	0.12	0.16	0.21	0.25	0.29	0.33	0.37	0.41	0.45	0.49	0.54	0.58	0.62	0.66

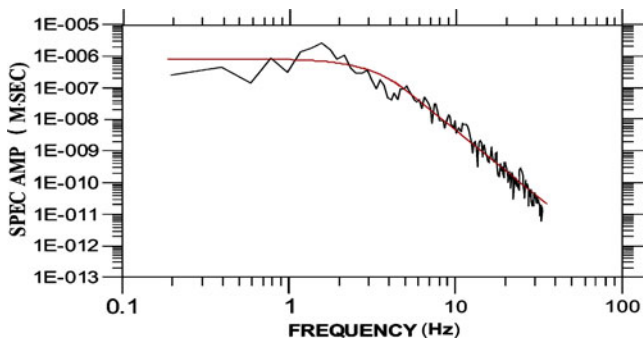
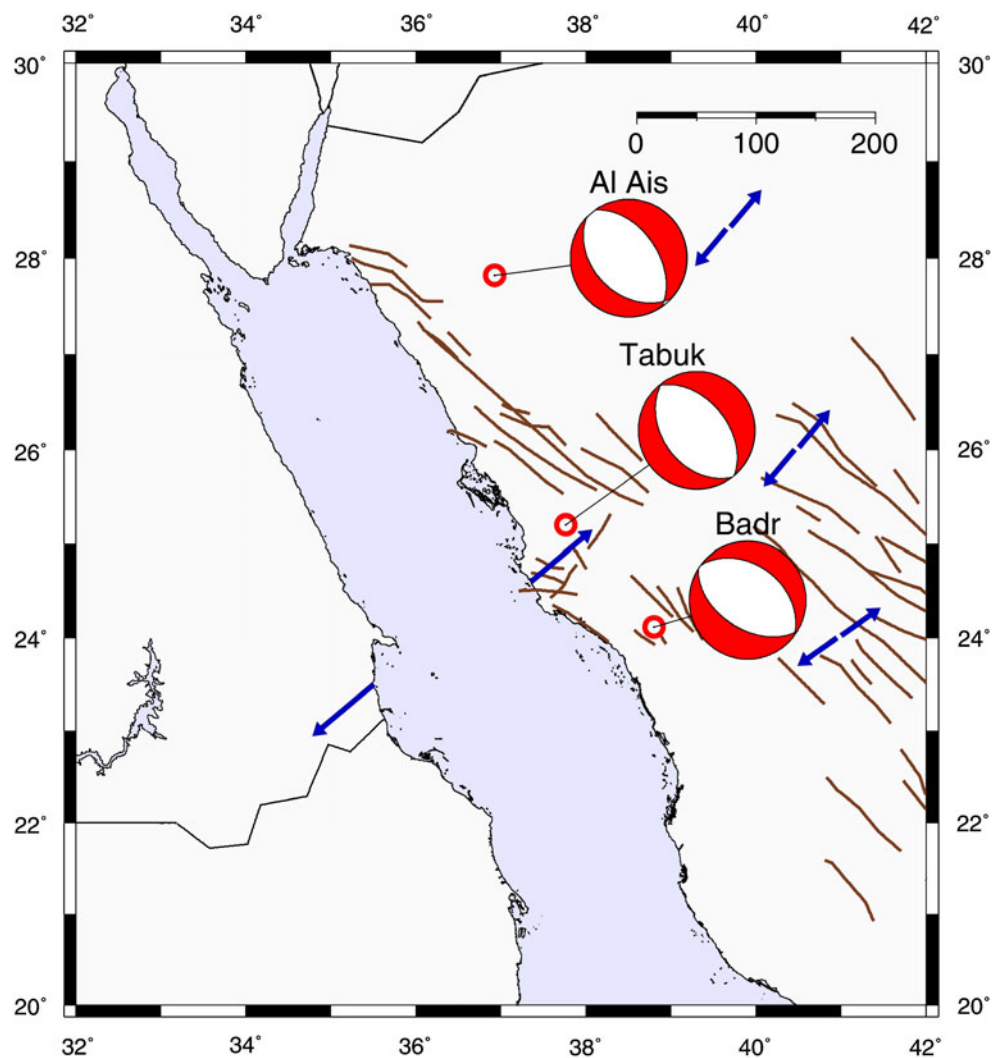


Fig. 4 Lg displacement spectra from KBRs stations for August 27, 2009, Badr earthquake. The *black line* indicates the spectrum while the *red* one indicates the fitted omega-square source model curve

(1) extensional boundary resulting from rifting and sea floor spreading in the Gulf of Aden and Red Sea in the south and west, thus creating new crust and embryonic oceanic basins; (2) compressional or collisional boundary, where two continental plate margins converge and collide, giving rise to an orogenic mountain chain, one plate; the Arabian plate

Fig. 5 The focal mechanism solutions of the three earthquakes located at the passive margin of the Red Sea and their stress pattern, Saudi Arabia



underriding the Eurasian plate to give rise to the Taurus and Zagros Mountains into the north and northeast and Oman Mountains in the southeast (where the collision occurs between a continental plate and an oceanic or a denser plate); this process shortens the plate edges by thickening and folding them; and (3) transform plate boundary in the west along the Levant (Dead Sea) fracture, where the plates slide past each other laterally without adding or destroying crustal material; here the Arabian plate is moving horizontally northward relative to the Sinai-Levantine plate, where horizontal displacement magnitudes in the southern sector of about 107 km can be measured by the distance offset of formerly contiguous features sliced by the Dead Sea fault zone (Quennell 1958, 1984).

GPS measurements (McClusky et al. 2003) indicate that the present-day motion of Arabian plate with respect to Nubian plate is 1.7–2.0 cm/year toward azimuth N 48° E. The GPS-derived velocity field for the zone of interaction of the Arabian, African, and Eurasian plates indicates counterclockwise rotation of the Arabian plate (Reilinger

et al. 2006). Counterclockwise rotation of the Arabian plate may be enhanced by slab pull from NE-directed subduction beneath the Makran and possibly the south Zagros. Rifting in the Red Sea and Gulf of Aden is a response to plate motions induced by active subduction. This interpretation implies that continuing subduction of the African and Arabian oceanic lithosphere is driving plate motions and interplate deformation throughout the zone of interaction of the African, Arabian, and Eurasian plates.

The causative source of the 27th August 2009 Badr earthquake is located along the Red Sea passive margin. This source area is characterized by low level of seismicity relative to the Red Sea extensional plate boundary where the recording of earthquakes is frequent. Historically, the area located 60 km NW of Badr has been experienced two moderate earthquakes. The existence of low to moderate earthquake activity is a typical for an intraplate earthquake zone in an extensional tectonic regime. The magnitude of Badr earthquake is too small to be well-recorded teleseismically. Consequently, it will not be included in the Global (Harvard) catalog. Therefore, local and regional seismic networks along the northern Red Sea margin must be used to determine the source mechanism of Badr earthquake. Since the beginning of the 1998, the countries bordering the northern Red Sea operated seismological networks. The two principal networks are the King Abdulaziz City of Science and Technology Seismic Network and the Egyptian National Seismological Network. The data of arrival times and polarities gathered from the seismological stations allowed relocation of Badr earthquakes with a better azimuthal coverage and computation of focal mechanisms using the HYPOINVERSE software (Klein 1987) and the crustal model of Rodgers et al. (1999). The epicenter of this event is 24.12° N and 38.79° E. The uncertainty for the Badr earthquake upon relocation is 0.56 km in epicentral location and 0.5 km in focal depth estimation. Based on the geological data, the location of this earthquake is very close to the NW-SE trending faults. The estimated local magnitude for this event is 3.8 ± 0.17 .

From the spectra of Lg waves recorded at four broadband stations the moment and moment magnitude for Badr earthquake were also calculated. Moment provides a better description of the real size of an earthquake. The average seismic moment and moment magnitude calculated from the displacement spectra of Lg waves for this event are $3.7e+14$ Nm and 3.66 ± 0.07 .

The estimated focal mechanism of Badr earthquake suggests pure normal faulting mechanism with the two nodal planes trending NW-SE. This trend seems to be correlated with the NW-SE trending faults in the area. The focal mechanism solution shows a dominant extensional regime with almost horizontal NE-SW trending *T*-axis.

Comparing the focal solution of Badr earthquake with the solutions of the 22th June 2004 ($M_w=5.1$) Tabuk and the 19th May 2009 ($M_w=5.7$) Al Ais earthquakes shows that the three earthquakes correspond to NW-SE normal faulting paralleling the Red Sea rift (Fig. 5). The *T*-axis orientations derived from the three earthquakes coincide pretty well with the prevailing NE-SW orientation of the regional extensional stress field resulting from the spreading in the Red Sea (Fig. 5). The NW-SE trending faults developed throughout the Arabian plate as a consequence of a NE-SW extensional stress regime (Eyal and Reches 1983). This stress system reactivated the pre-existing lineaments of the Najd fault system, which was active during the Precambrian, and was reactivated several times during the geological history of the region (Agar 1987; Hussein 1988; Stern 1994). The above results agree well with the geological investigations (Roobol 2007) which show that Red Sea passive margin is undergoing extension by rotational normal faulting dipping both towards and away from the Red Sea that cause thinning of the Arabian Shield.

References

- Agar RA (1987) The Najd fault system revisited; a two-way strike-slip orogen in the Saudi Arabian shield. *J Struct Geol* 9:41–48
- Aldamegh KS, Abou Elenean KM, Hussein HM, Rodgers AJ (2009) Earthquake sequence, Eastern Red Sea margin, Kingdom of Saudi Arabia. *J Seismol*. doi:10.1007/s10950-008-9148-5
- Ambraseys NN, Melville CP, Adams RD (1994) The seismicity of Egypt, Arabia and the Red Sea: a historical review. Cambridge University Press, Cambridge
- Beydoun ZR (1994) Arabian plate oil and gas: why so rich and so prolific? *Episodes* 21(2):74–81
- Camp VE (1984) Island arcs and their role in the evolution of the western Arabian Shield. *Geol Soc Am Bull* 95:913–921
- Camp VE, Hooper PR, Roobol MJ, White DL (1987) The Madinah historical eruption, Saudi Arabia: magma mixing and simultaneous extrusion of three basaltic chemical types. *Bull Volcanol* 49:489–508
- Delfour J (1983) Geology and mineral resources of the northern Arabian Shield. Saudi Arabian Deputy Minist. Miner. Resour. *OpenFile Rep.* BRGMOF0230
- Ebel John E (1982) M_L measurements for northeastern United States earthquakes. *Bull Seismol Soc Am* 72(4):1367–1378
- Eyal Y, Reches Z (1983) Tectonic analysis of the Dead Sea Rift region since the late-Cretaceous based on mesostructures. *Tectonics* 2:167–185
- Hussein MI (1988) The Arabian infracambrian extensional system. *Tectonophysics* 148(1–2):93–103
- Johnson PR (1983) A preliminary lithofacies map of the Arabian Shield. Deputy Ministry of Mineral Resources, Jeddah, Saudi Arabia, Technical Record RF-TR-03-2, p 72
- Klein RW (1987) Hypocenter location program. HYPOINVERSE, part 1:user guide, open file report. US Geological Survey, Menlo Park, p 113
- McClusky S, Reilinger R, Mahmoud S, Ben Sari D, Tealeb A (2003) GPS constraints on Africa (Nubia) and Arabia plate motions. *Geophys J Int* 155:126–138
- Nuttli OW (1973) Seismic wave attenuation and magnitude relations for eastern North America. *J Geophys Res* 78:876–885

- Quennell AM (1958) The structural and geomorphic evolution of the Dead Sea Rift. *Q J Geol Soc Lond* 114:1–24
- Quennell AM (1984) The western Arabian rift system. In J.E. Dixon and A.R.F. Robertson eds, the Geological Evolution of the eastern Mediterranean. Geological Society Special Publication 17:775–788
- Reilinger R, McClusky S, Vernant P, Lawrence S, Ergintav S, Cakmak R, Ozener H, Kadirov F, Guliev I, Stepanyan R, Nadariya M, Hahubia G, Mahmoud S, Sakr K, ArRajehi A, Paradissis D, Al-Aydrus A, Prilepin M, Guseva T, Evren E, Dmitrotsa A, Filikov SV, Gomez F, Al-Ghazzi R, Karam G (2006) GPS constraints on continental deformation in the Africa-Arabia-Eurasia continental collision zone and implications for the dynamics of plate interactions. *Journal of geophysical research* 111:1–26. doi:10.1029/2005JB004051, B05411
- Richter CF (1958) Elementary seismology. W. H. Freeman, San Francisco, p 758
- Richter CF (1935) An instrumental earthquake magnitude scale. *Bull Seismol Soc Am* 25:1–32
- Rodgers A, Walter WR, Mellors RJ, Abdullah MS, Al-Amri, Zhang Y-S (1999) Lithospheric structure of the Arabian shield and platform from complete regional waveform modelling and surface wave group velocities. *Geophys J Int* 138:871–878
- Roobol J (2007) Cenozoic faults in Western Saudi Arabia. In: 7th meeting of the Saudi society for geosciences, King Saud University, Riyadh, Saudi Arabia
- Sandvol Eric A, Bao Xueyang, Ekrem Zor, Jiakang Xie, Brian J, Mitchell, David P. Schaff (2007) Lg and pg attenuation in the middle east. 29th Monitoring Research Review: Ground-Based Nuclear Explosion Monitoring Technologies, 266–273
- Snoke A (2003) Focal mechanism determination software (FOCMEC package), <http://www.geol.vt.edu/outreach/vtso/focmec>
- Stern R (1985) The Najd fault system, Saudi Arabia and Egypt: a late Precambrian rift-related transform system? *Tectonics* 4(5):497–511
- Stern RJ (1994) Arc assembly and continental collision in the Neoproterozoic East African orogen: implications for the consolidation of Gondwanaland. *Annual Review of Earth and Planetary. Science* 22:319–351
- Stoeser DB (1986) Distribution and tectonic setting of plutonic rocks of the Arabian Shield. *J Afr Earth Sci* 4:21–46
- Stoeser DB, Fleck RJ, Stacey JS (1984) Geochronology and origin of early tonalite gneiss of the WADI Tarib batholith and the formation of syn-tectonic gneiss complexes in the southeast Arabian Shield. *Faculty Earth Science Bulletin, King Abdulaziz University, Jeddah* 6,351–364
- Street RL, Herrmann RB, Nuttli OW (1975) Spectral characteristics of the Lg-wave generated by the central United States earthquakes. *Geophys J R Astron Soc* 41:51–63
- Vail JR (1983) Pan-African crustal accretion in northeast Africa. *J Afr Earth Sci* 1:285–294